




# Joint Correction of Tropospheric and Orbital Errors in SAR Differential Interferograms

*Correcção Conjunta de Erros Troposféricos e Orbitais nos Interferogramas Diferenciais SAR*

Kamel Hasni<sup>1</sup> , Bachir Gourine<sup>1</sup> , Houaria Namaoui<sup>1</sup> , Mohammed El Amin Larabi<sup>1</sup>  & Saddam Housseyn Allal<sup>1</sup> 

<sup>1</sup>Centre des Techniques Spatiales, Agence Spatiale Algérienne, Arzew, Algérie 01, av. de la Palestine, 31200 - Arzew, Algeria  
E-mail: khasni@cts.asal.dz, hasni.kamel@gmail.com

## Abstract

Synthetic Aperture Radar (SAR) satellite imagery is a source of data widely employed in the quantification and analysis of an earthquake coseismic displacement. However, due to the signal path along the atmosphere and to other sources, the interferometric phase becomes compromised. In this work, a methodology for the correction of tropospheric and orbital errors in the differential interferogram is presented. This methodology was applied to a couple of Sentinel-1A data. The phenomenon studied was the 11<sup>th</sup> November 2018 Zeribet el Oued earthquake, Mw. 5.2 (The state of Biskra, South East of Algeria). It was possible to correct both tropospheric and orbital errors, where the dominant one was the tropospheric delay, a displacement error of 4 cm was added to the differential interferogram by this noise source. The correction of orbital error led to a better interpretation of the coseismic displacement.

**Keywords:** Tropospheric path delay; Orbit error correction; DInSAR

## Resumo

Imagens de satélite *Synthetic Aperture Radar* (SAR) são uma boa fonte de dados usados na quantificação e análise do deslocamento cossísmico do terremoto. Porém, devido ao caminho do sinal ao longo da atmosfera e a outras fontes, a fase interferométrica fica comprometida. Neste trabalho, é apresentada uma metodologia para a correção de erros troposféricos e orbitais no interferograma diferencial. Esta metodologia foi aplicada a alguns dados do Sentinel-1A, o fenômeno estudado foi o terremoto Zeribet el Oued de 11 de novembro de 2018, Mw. 5.2 (O estado de Biskra, sudeste da Argélia). Foi possível corrigir os erros troposférico e orbital, onde o dominante era o atraso troposférico, um erro de deslocamento de 4 cm foi adicionado ao interferograma diferencial por esta fonte de ruído. A correção do erro orbital permitiu uma melhor interpretação do deslocamento cossísmico.

**Palavras-chave:** Atraso do caminho troposférico; Correção de erro de órbita; DInSAR

# 1 Introduction

Since the success in coseismic displacement mapping of the 1992 Landers earthquake (Mw 7.3), by ERS-1 satellite radar images using the interferometric technique, Differential Interferometric Synthetic Aperture Radar (DInSAR) has become a viable mean for the study of land surface displacement caused by natural hazards (earthquakes, volcano eruptions, landslides, etc...) (Burgman, Rosen & Fielding 2000; Hanssen 2001). Using InSAR data to detect and study earthquakes has numerous advantages over other techniques, and this is related to the capacity of imaging by day and night-time and even at extreme atmospheric conditions.

DInSAR technique provides measurements in one direction following the signal illumination path, which is called Line-Of-Sight (LOS). Based on LOS information, it is possible to acquire more accurate measures of earthquake location than teleseismic methods (Weston, Ferreira & Funning 2011) and denser observations comparing to a GPS network (Xiao & He 2013). Furthermore, it is possible to retrieve the full 3-D displacement vector from the combination of two interferometric couples (ascending and descending) or using information from the Along Track direction like Offsets Tracking or Multiple Aperture Interferometry (MAI) (Jung, Won & Kim 2009; Michel, Avouac & Taboury 1999). While DInSAR has improved the ability to study quite a number of geophysical phenomena, it is not always possible to get useful information. The interferometric phase may be hidden or destroyed by the presence of errors and noise sources. A better interpretation of a studied phenomenon requires results with high precision; thus, errors should be accounted for and reduced.

Error sources in DInSAR can be divided into: geometric, atmospheric, and temporal categories (Massonnet & Feigl 1998). Geometric sources are the result of a large orbital separation impeding the construction of the interferometric phase (Xu et al. 2014). Moreover, errors related to the topography removal are caused by the presence of shadow or layover, etc. (Massonnet & Feigl 1998). Atmospheric errors; in another hand, can be a result of a turbulent troposphere or an ionospheric anomaly (Ding et al. 2008; Meyer et al. 2006), causing a delay in the radar path. Such an error occurs in the case of a difference in the atmospheric conditions between the two SAR acquisitions, leading to a differential atmospheric phase in the interferogram.

In this work, a method for the correction of tropospheric and orbital errors is presented. Tropospheric correction is achieved with the help of the European Center for Medium-Range Weather Forecasts (ECMWF) global weather model with a high-resolution grid. A second correction is employed for the reduction of orbital noise;

which is computed by the mean of a 2-D polynomial function where the coefficients are estimated by the least-squares method. The present paper is structured as follows: In Section 2, the tropospheric and orbital correction method is described in details. The data used for the study and the results obtained are discussed, in Section 3.

## 2 Methodology

### 2.1 Tropospheric Correction

Atmospheric Phase Screen (APS) is a common issue to the DInSAR technique; since radar signals travels through the troposphere. It is caused by changes in the refractive index in the atmosphere between the acquisitions. Formally, tropospheric artifacts can be decomposed into two distinct categories; turbulent and stratified (Ding et al. 2008; Hanssen et al. 1999; Hu et al. 2014). Both of them limit the accuracy of deformation retrieval in the LOS direction. The stratified effect takes its name from the stratification of the atmosphere appearing between different vertical refractivity layers. It is correlated with topographic height (Biggs et al. 2007, Doin & al. 2009; Remy et al. 2003) causing a delay in mountainous areas. One way to correct this artifact is by considering linear or quadratic regression. Other advanced methods are used; like multi-scale or multi-resolution analysis (Lin et al. 2010; Shirzaei & Burgmann 2012). However, these methods cannot correct the turbulent artifacts, resulting from the variation of water vapor in the lower troposphere. The best way to eliminate such, an error from the interferogram is to use available external data; like ground-based meteorological measurements (Delacourt, Briole & Acchache 1998), Global Positioning System (GPS) observations (Li et al. 2004), that can be combined with near infra-red spectrometers as MODIS or MERIS (Li, Ding & Li 2004). Nowadays, because of the spatial and temporal resolutions and the increased accuracy, the most used method for the correction is by simulating the tropospheric artifacts based on the Numerical Weather Models (NWM) (Jolivet et al. 2011).

The 2-way tropospheric phase delay,  $\varnothing_{tropo}$  at specific height  $h=h_1$ , corresponds to the integration of the hydrostatic and wet component of the refractivity  $N$  between  $h_1$  and the top of the troposphere  $h_{top}$  along the radar LOS as:

$$N = \left( k_1 \frac{P}{T} \right)_{hydr} + \left( k_2 \frac{e}{T} + k_3 \frac{e}{T^2} \right)_{wet} = N_{hydr} + N_{wet} \quad (1)$$

$$\varnothing_{tropo} = \frac{-4\pi}{\lambda} \frac{10^{-6}}{\cos\theta} \int_{h_1}^{h_{top}} (N_{hydr} + N_{wet}) dh \quad (2)$$

Where  $P$  indicates atmospheric pressure,  $T$  the temperature,  $e$  the partial pressure of water vapor,  $\theta$  the incidence angle,  $\lambda$  the radar wavelength, and  $\frac{-4\pi}{\lambda}$  a conversion factor to convert from pseudo-range increase to phase delay. The coefficients  $k_1$ ,  $k'_2$ ,  $k_3$  and are empirical constants that are taken as:  $k_1 = 77.6 \text{ K hPa}^{-1}$ ,  $k'_2 = 23.3 \text{ KhPa}^{-1}$ , and  $k_3 = 3.75 \cdot 10^5 \text{ K}^2 \text{ hPa}^{-1}$ . For DInSAR, the interferometric tropospheric phase delay  $\Delta\phi_{\text{tropo}}$  referred to as Atmospheric Phase Screen (APS) corresponds to the difference between tropospheric delays at the master and slave acquisition times  $\Delta\phi_{\text{tropo}} = \phi_{\text{tropo}}^{\text{slv}} - \phi_{\text{tropo}}^{\text{mst}}$ , and thus depends on the change in refractivity, rather than the total refractivity.

The output (pressure, temperature, and relative humidity) from local or global weather models can be used with Equation 1 to compute both hydrostatic and wet tropospheric delays. A direct integration method is used to integrate the stratified delay along the path using a 4-dimensional global Numerical Weather Prediction product ERA5 data provided from the (ECMWF). The integration starts from a given point; then meteorological parameters at each integration step are interpolated or extrapolated along the integration path in the slant range direction.

## 2.2 Correction of Orbital Errors

The trajectory of a SAR satellite is difficult to be precisely modeled, so in a consequence the interferometric baseline. A precise orbit can be determined at the centimetric level (Scharroo & Visser 1998). Therefore, the flat earth phase removing is incomplete, and they're still a residual ramp left in the interferometric phase. Besides, the inaccurate baseline would lead to an incomplete topographic contribution removal when generating a differential interferogram. These errors must be removed for high precision deformation measurements. A second-degree polynomial is used for the estimation of the orbital error (Hasni, Chen & Wei 2017; Xu et al. 2014). This model takes into account the residual topographic inaccuracy, introduced by the external Digital Elevation Model (DEM) used to remove the topography from the interferogram. This residual error is altitude dependent and the model can be expressed as:

$$\varnothing^{\text{orb}}(x, y) = a_0 + a_1x + a_2y + a_3xy + a_4x^2 + a_5y^2 + a_6h(x, y) \quad (3)$$

Where  $\varnothing^{\text{orb}}$  states for the orbital and residual topography errors,  $a_{0-6}$  are model parameters,  $x$  and  $y$  are coordinates of the pixel in the interferogram, and  $h(x, y)$  denotes the altitude of the pixel, it can be extracted from the DEM. A sufficient number of points outside the displacement area should be used and a robust regression using reweighted Least-Squares is performed for a proper estimation of model

parameters. This joint correction of tropospheric and orbital errors deals first with the tropospheric phase delay. Since the application of the non-linear model can deal with a part of the tropospheric delay as an orbital error.

## 2.3 InSAR Processing

The interferometric processing is done using GMTSAR software (Sandwell et al. 2011). It is a flexible tool offering two choices; the entire interferometric processing can be run in the automatic mode; starting from RAW or Single Look Complex (SLC) images (depending on the data), until the generation of geocoded results. Manual processing is possible too, where each step is performed individually if the user is willing to change some parameters. GMTSAR software is based on Generic Mapping Tools (GMT) GIS software (Wessel & Smith 1998), used from the DEM coregistration step until the end of the processing. The unwrapping step was done using Snaphu software (Chen & Zebker 2000).

## 3 Results and Discussion

The combined correction of tropospheric and orbital delays was applied to correct the errors in the differential interferogram generated for the study of the 5.2 Mw earthquake that struck near the area of Zeribet El Oued (Biskra-Algeria) on 18<sup>th</sup> November 2016 at 08<sup>h</sup>42<sup>m</sup> local time. For this purpose, two images from the European Satellite Sentinel-1A TOPS data of the Track 66 in the descending mode is used (Figure 1).

A 12 days' couple is used, this temporal separation helps to reduce error sources, the master image was taken on the date of November 28, and the slave on November 16<sup>th</sup> 2016. The interferogram was generated using GMTSAR version 5.6 and GMT compatible version 5.3.1, the topographic phase was reduced with a 90 m Shuttle Radar Topography Mission (SRTM) DEM version 4 (Farr et al. 2007). Figure 2 shows the coherence image of the interferogram. This couple shows a high coherence with a mean of 0.69 and a maximum of 0.97, this coherence level helps the phase unwrapping because it reduces the phase noise.

In this test the perpendicular baseline ( $B_{\perp}$ ) is equal to 19.43 m, this leads to an altitude of ambiguity of 820.3m, such kind of configuration is favorable for DInSAR applications since the interferogram is not sensitive to the topography (1 topographic fringe every 820.3 m). However, tropospheric errors can be present in the interferograms if the atmospheric conditions are different at the two acquisition times. The interferogram resulting from the processing is presented in Figure 3A, and the corresponding Line-Of-Sight (LOS) displacement by Figure 4A.

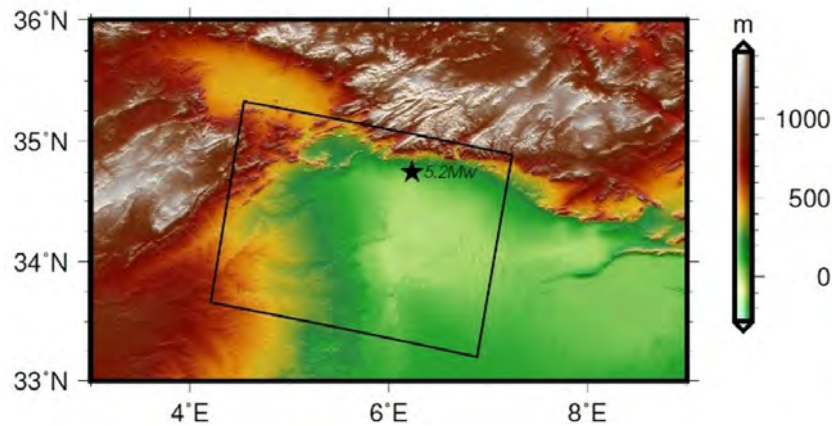


Figure 1 Shaded relief map covering the study area. The star indicates the earthquake epicenter. The black rectangle represents the Sentinel-1 Track 66 descending scene used for the study of the 18 November 2016 earthquake

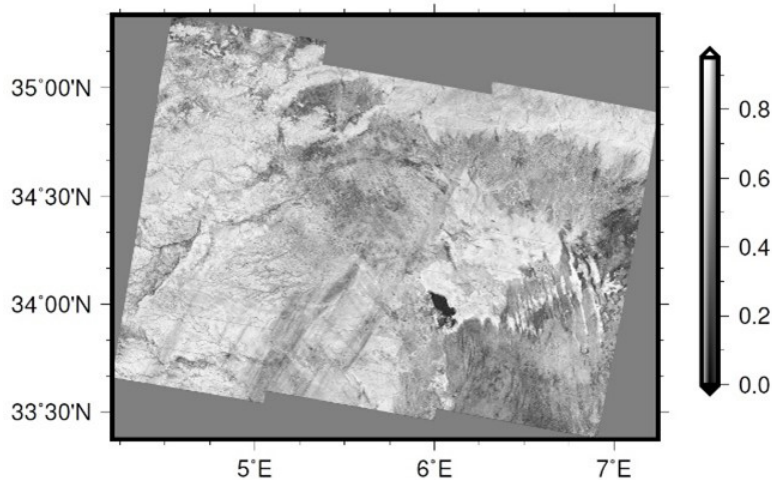


Figure 2 Coherence image of the interferometric couple.

The preliminary analysis shows clearly two distinguished fringes in the differential interferogram (Figure 3A), meaning at least 6 cm of land movement. The LOS presented in Figure 4A shows a displacement varying from -6 cm to +4 cm, so it is in the range of 10 cm. This kind of displacement is difficult to map in the case of an earthquake of magnitude 5.2 and a depth of 26 km. In Funning & Garcia (2019), simulations showed that an intraplate 5.5 Mw event with a depth of 10 km can produce no more than 22 mm of displacement in extreme cases, so we should not expect more than 3 cm of displacement for our case. Following these considerations, an investigation of external error sources is started to better interpret this land movement.

The first considered error is the tropospheric phase delay, in Figure 4B is presented the differential tropospheric path delay in centimeters, and in Figure 3B is shown the wrapped tropospheric phase. The differential tropospheric delay is between -4.5 cm to 0.5 cm, meaning that this value is added to the differential interferogram and interpreted as displacement rather than noise if not corrected. For a better understanding of this error range, the tropospheric delay is converted to an unwrapped phase then wrapped to get the fringe pattern visible in Figure 3B.

The tropospheric error presented in Figure 4B shows how big is that noise source in the displacement interpretation. The corrected LOS from the tropospheric path delay is shown in Figure 4C. It is worth mentioning,

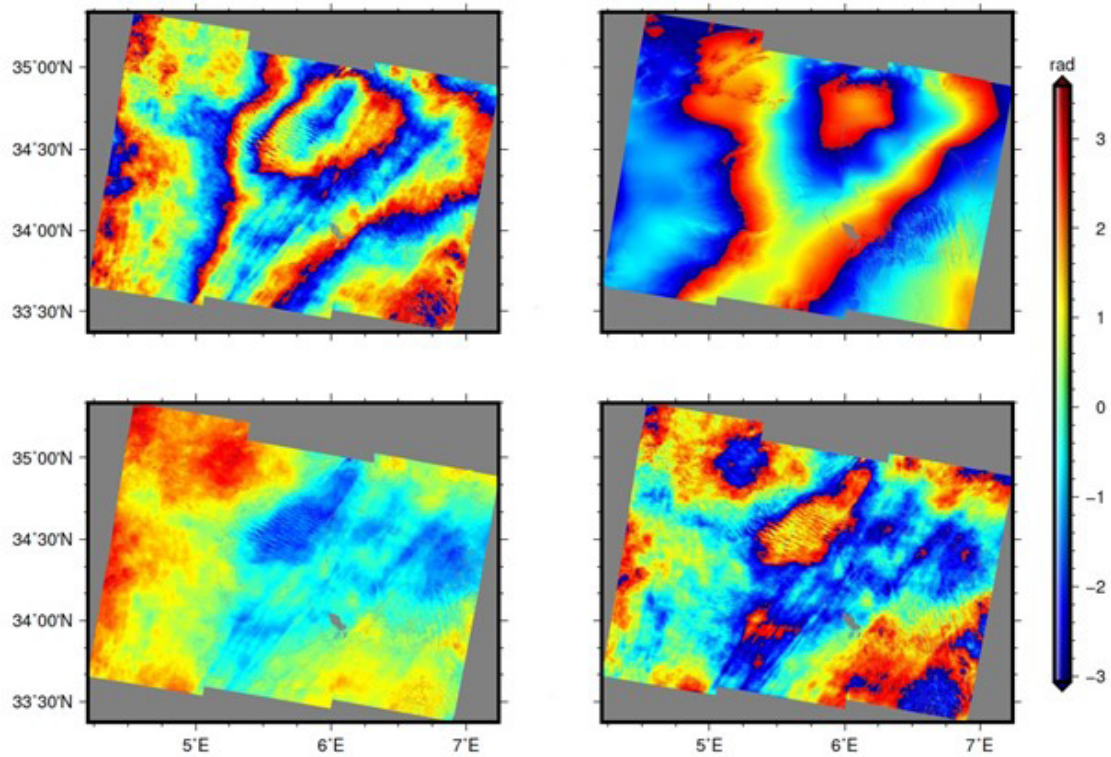


Figure 3 Results of the tropospheric correction: A. original interferogram; B. wrapped tropospheric phase; C. corrected interferogram; D. corrected interferogram after linear trend removal.

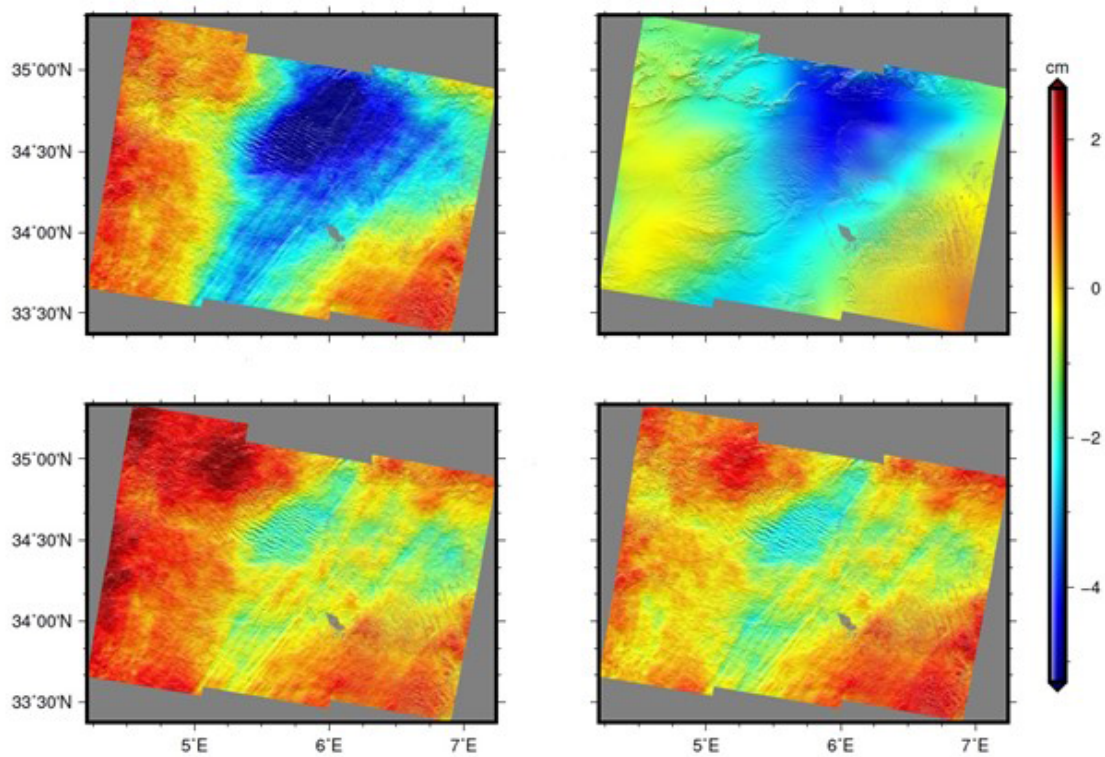


Figure 4 Line-Of-Sight tropospheric correction; A. Original LOS in cm; B. tropospheric delay estimated from ERA-5 data; C. corrected interferogram from the tropospheric delay; D. LOS after the correction from the tropospheric and linear trend.

that if a linear trend is present in the interferogram, a correction can be done as shown in Figures 3D and 4D for the wrapped and unwrapped corrections respectively. The analysis of Figure 3B, confirms that the mapped LOS displacement is noisy, and this is related to the presence of at least one and half of a fringe considered as an error rather than displacement. The fringe structure in the tropospheric phase has the same pattern as the displacement fringe in the interferogram. Meaning that it has no relation with the displacement, but it is an error that should be corrected. It is really rare to get such a tropospheric fringe structure. The topography of the region and the arid climate (desert area)

could be a possible reason for that. Further exploration of error sources led to the investigation of orbital and residual topographic ones. The estimated orbital phase error is presented in Figure 5.

Finally, the correction of orbital error shows a less apparent movement as presented in Figure 6. Accordingly, to the orbital phase error presented in Figure 5, the phase range is between -2.5 to 2 radian, translated to a displacement error varying from -1.1 to 1.5 cm. Such an error can lead to a misinterpretation of the movement, especially in this case where the expected displacement should be small.

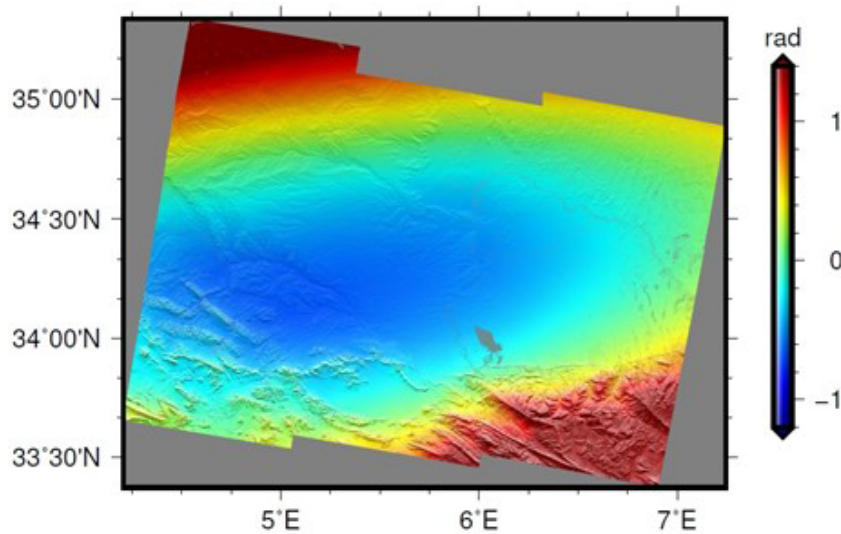


Figure 5 Orbital error affecting the interferogram, the main bias is concentrated at the center of the scene and at the top left and the bottom right.

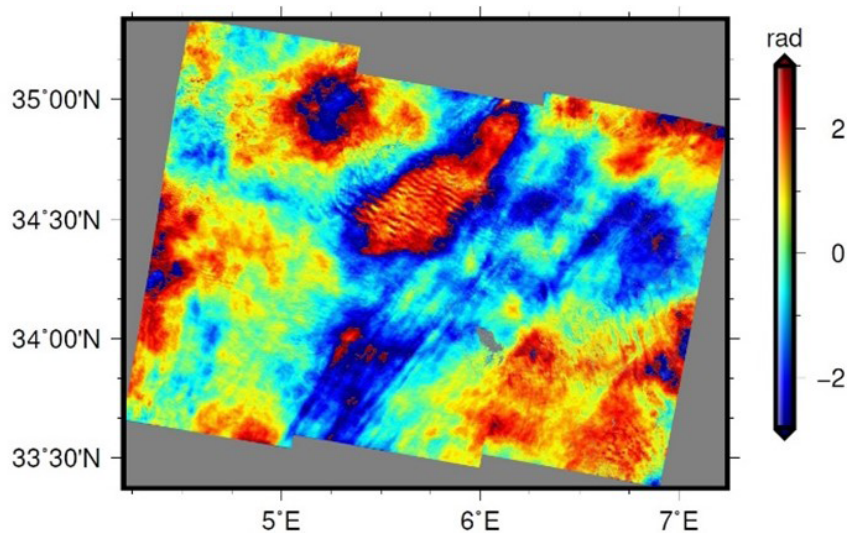


Figure 6 Tropospheric and orbital free interferogram showing a big improvement after the correction.

Five profiles across the LOS are plotted for different levels of correction (see Figure 7). In the first profile, the original phase reached the value of -6 cm (black solid line), the tropospheric corrected phase (red line) varies from -2 cm to 2 cm, and a difference of 1.5 to -0.5 cm is noticed after orbital correction (blue line). The same interpretation can be addressed to the profiles from 2 to 5,

where the tropospheric and orbital errors become closer to each other when moving south of the displacement area. The five profiles show a LOS reaching -7 cm before any correction. However, the final corrected LOS is varying from -2 to 2 cm, it is an improved measurement for the displacement caused by the Zeribet EL Oued earthquake, especially where no surface damages were observed.

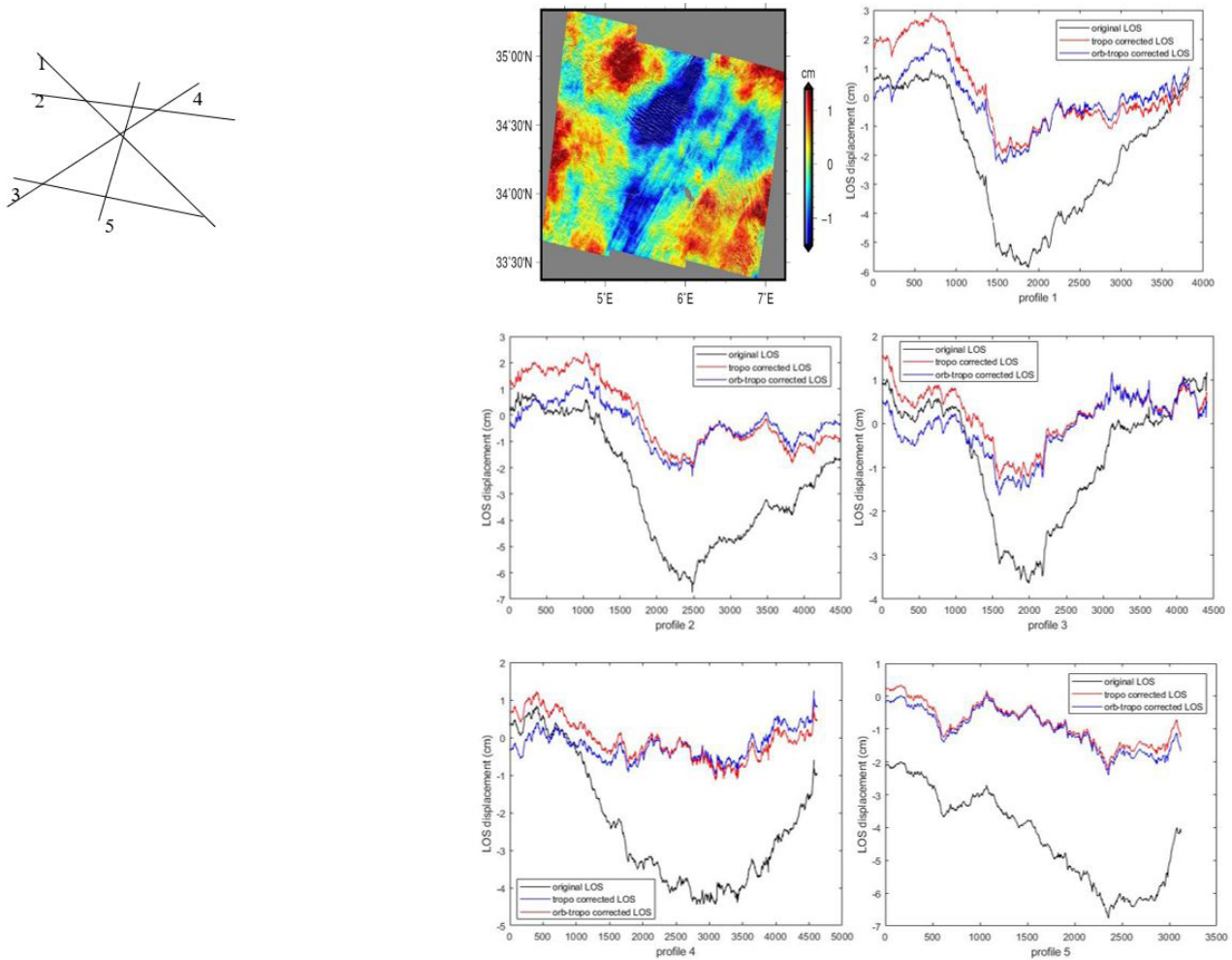


Figure 7 Arbitrary profiles in different directions. A. At the top left, the LOS corrected from the tropospheric and orbital errors, the lines represent the profiles. B. The five profiles, the black solid line represents the profiles of the original LOS in cm, the red for the tropospheric correction, and the blue for the tropospheric and orbital correction.

## 4 Conclusion

In this work, a joint correction for tropospheric and orbital errors in a differential interferogram is presented. The theoretical background was presented in Section 2 and the processing results were discussed in Section 3. The application of this methodology on a coseismic interferogram of a 5.2 Mw earthquake, in the region of Zeribet el Oued, Algeria, showed a big improvement of the displacement information after the correction. The tropospheric path delay was dominant in the interferogram, where two visible fringes were added to the differential interferogram, leading to a misinterpretation of the displacement information. On another hand, the orbital errors ranging from -1.1 to 1.5 cm, are considered as another biasing source. The improvement of this combined correction was verified by the arbitrary profiles taken in different regions of the interferogram. Good displacement information is required for geodetical and geophysical interpretation, and error sources should be accounted for, to a better understanding of the earthquake mechanism.

## 5 References

- Biggs, J., Wright, T.B., Lu, Z. & Parsons, B. 2007, 'Multi-Interferogram Method for Measuring Interferometric Deformation: Denali Fault, Alaska', *Geophysics Journal International*, vol. 170, no. 3, pp. 1165-79.
- Burgman, R., Rosen, P.A. & Fielding, E.J. 2000, 'Synthetic Aperture Radar Interferometry to Measure Earth's Surface Topography and Its Deformation', *Annual Review of Earth and Planetary Sciences*, vol. 28, pp. 169-209.
- Chen, C.W. & Zebker, H.A. 2000, 'Network approaches to two-dimensional phase unwrapping: intractability and two new algorithms', *Journal of the Optical Society of America*, vol. 17, no. 3, pp. 401-14.
- Delacourt, C., Briole, P. & Acchache, J. 1998, 'Tropospheric Correction of SAR Interferograms With Strong Topography', *Geophysical Research Letter*, vol. 25, no. 15, pp. 2849-52.
- Ding, X.L., Li, Z.W., Zhu, J.J., Feng, G.C. & Long, J.P. 2008, 'Atmospheric Effects on InSAR Measurements and Their Mitigation', *Sensors*, vol. 8, no. 9, pp. 5426-48.
- Doin, M.-P., Lassere, C., Peltzer, G., Cavalié, O. & Dobre, C. 2009, 'Correction of Stratified tropospheric Delays in SAR Interferometry: Validation with Global Atmospheric Models'. *Journal of Applied Geophysics*, vol. 69, no. 1, pp. 35-50.
- Farr, T., Rosen, P.A., Caro, E., Crippen, R., Duren, R., Hensley, S., Kobrick, K., Paller, M., Rodriguez, E. & Roth, L. 2007, 'The shuttle Radar Topography Mission', *Reviews of Geophysics*, vol. 45, no. 2, pp. 1-33.
- Funning, G.J. & Garcia, A. 2019, 'A systematic study of earthquake detectability using Sentinel-1 Interferometric Wide-Swath data', *Geophysical Journal International*, vol. 216, no. 1, pp. 332-49.
- Hanssen, R.F., Weckwerth, T.M.E., Zebker, H.A. & Klees, H.A. 1999, 'High-Resolution Water Vapor Mapping From Interferometric Radar measurements', *Science*, vol. 283, no. 5406, pp. 1297-9.
- Hanssen, R.F. 2001, *Radar Interferometry: Data Interpretation and Error Analysis*, Kluwer Academic Publishers, Dordrecht, Boston.
- Hasni, K., Chen, J. & Wei, G. 2017, 'Correcting Ionospheric and Orbital Errors in Spaceborne SAR Differential Interferograms', *IEEE International Conference on Imaging Systems and Techniques (IST)*, Beijing, pp.1-5.
- Hu, J., Li, Z.W., Ding, X.L., Zhua, J.J., Zhang, L. & Suna, Q. 2014, 'Resolving Three Dimensional Surface Displacements from InSAR Measurements: A Review', *Earth Science Reviews*, vol. 133, pp. 1-17.
- Jolivet, R., Grandin, R., Lassere, C., Doin, M.P. & Peltzer, G. 2011, 'Systematic InSAR Tropospheric Phase Delay Corrections From Global Meteorological Reanalysis Data', *Geophysical Research Letter*, vol. 38, no. L17, pp. L17 311-1 L17 311-6.
- Jung, H.S., Won, J.-S. & Kim, S.-W. 2009, 'An Improvement of the Performance of Multiple-Aperture SAR Interferometry (MAI)'. *IEEE Transactions on Geoscience and Remote Sensing*, vol. 47, no. 8, pp. 2859-69.
- Li, Z.W., Ding, X.L. & Li, G. 2004, 'Modeling Atmospheric Effects on InSAR GPS Observations: Algorithms and Some Test Results', *Journal of Atmospheric and Solar-Terrestrial Physics*, vol. 66, no. 11, pp. 907-17.
- Lin, Y.N., Simons, M., Hetland, E.A., Muse, P. & Dicaprio, C. 2010, 'A Multiscale Approach to Estimating Topographically Correlated Propagation Delays in Radar Interferograms', *Geochemistry Geophysics Geosystems*, vol. 11, no. 9.
- Massonnet, D. & Feigl, K.L. 1998, 'Radar Interferometry and Its Application to Changes in the Earth's Surface', *Review of Geophysics*, vol. 36, no. 4, pp. 441-500.
- Meyer, F., Bamler, R., Jakowsky, N. & Fritz, T. 2006, 'The Potential of Low-Frequency SAR Systems for Mapping Ionospheric TEC Distributions', *IEEE Geoscience and Remote Sensing Letters*, vol. 3, no. 4, pp. 560-4.
- Michel, R., Avouac, J.P. & Taboury, J. 1999, 'Measuring Ground Displacements from SAR Amplitude Images: Application to the Landers Earthquake', *Geophysical Research Letter*, vol. 26, no. 7, pp. 875-8.
- Remy, D., Bonvalot, S., Briole, P. & Murakami, M. 2003, 'Accurate Measurements of tropospheric Effects in Volcanic Areas From SAR Interferometry Data: Application to Sakurajima Volcano (Japan)', *Earth Planet Science Letter*, vol. 213, no. 3-4, pp. 299-310.
- Sandwel, D., Mellors, R., Tong, X., Wei, M. & Wessel, P. 2011, 'Open radar Interferometry Software for Mapping Surface Deformation', *EOS Transactions, American Geophysical Union*, vol. 92, no. 28.
- Scharroo, R. & Visser, P. 1998, 'Precise Orbit Determination and Gravity Field Improvement for the ERS Satellites', *Journal of Geophysical Research*, vol. 103, no. 4, pp. 8113-27.
- Shirzaei, M. & Burgmann, R. 2012, 'Topography Correlated Atmospheric Delay Correction in Radar Interferometry Using



- Wavelet transforms', *Geophysical Research Letter*, vol. 39, no. 1, pp. L01 305-1-L01 305-6.
- Wessel, P. & Smith, W.H.F. 1998, 'New Improved version of the Generic Mapping Tools Released', *EOS Transactions, American Geophysical Union*, vol. 79, no. 579.
- Weston, J., Ferreira, A.M.G. & Funning, G.J. 2011, 'Global compilation of interferometric synthetic aperture radar earthquake source models: 1. Comparisons with seismic catalogs', *Journal of Geophysical Research Atmospheres*, vol. 116, pp. B08408.
- Xiao, R. & He, X. 2013, 'GPS and InSAR Time Series Analysis: Deformation Monitoring Application in a Hydraulic Engineering Resettlement Zone, Southwest China', *Mathematical Problems in Engineering*, vol. 601209, pp. 1-11.
- Xu, B., Li, Z., Wang, Q., Jian, M., Zhu, J. & Ding, X. 2014, 'A Refined Strategy for Removing Composite Errors of SAR Interferograms', *IEEE Geoscience and Remote Sensing Letters*, vol. 1, no. 1, pp. 143-7.

Received: 4 October 2020

Accepted: 3 August 2021

### How to cite:

Hasni, K., Gourine, B., Namaoui, H., Larabi, M.E.A. & Allal, S.H. 2021, 'Joint Correction of Tropospheric and Orbital Errors in SAR Differential Interferograms', *Anuário do Instituto de Geociências*, vol. 44: 38730. [https://doi.org/10.11137/1982-3908\\_2021\\_44\\_38730](https://doi.org/10.11137/1982-3908_2021_44_38730)